LIMNOLOGY
and
OCEANOGRAPHY

ASLO

Limnol. Oceanogr. 62, 2017, 973–988

doi: 10.1002/lno.10479

Dynamics and production of dissolved organic carbon in a large continental shelf system under the influence of both river plume and coastal upwelling

Kai Wu,[1] Minhan Dai,[1]* Xiaolin Li,[1] Feifei Meng,[1] Junhui Chen,[1] Jianrong Lin[2]
[1]State Key Laboratory of Marine Environmental Science, Xiamen University, Xiamen, China
[2]Department of Environmental Science and Engineering, Xiamen University Tan Kah Kee College, Zhangzhou, China

Abstract

We examined the dynamics and production of dissolved organic carbon (DOC) on a large continental shelf in the northern South China Sea, which is largely shaped by a river plume and coastal upwelling, based on a cruise in summer 2008. The plume water extended from the mouth of the Pearl River estuary to the middle shelf and was characterized by high DOC concentrations, while the upwelled water occupying the nearshore area featured low DOC concentrations. Biological production of DOC was observed in both the river plume and the coastal upwelling zones with different behavior between regions. The system appeared to be autotrophic in terms of DOC throughout the plume, while in the upwelling circulation, the metabolism of DOC was mixed trophic. Nevertheless, the integrated net DOC production rate of 11.5 ± 6.9 mmol C m^{-2} d^{-1} in the upwelling zone was comparable to that in the plume (7.1 ± 7.0 mmol C m^{-2} d^{-1}). The net DOC production correlated strongly with net consumption of dissolved inorganic carbon (DIC) and inorganic nutrients, suggesting that the net DOC production was highly coupled to net community production (NCP) in both the plume and upwelling zones. Both regimes had similar DOC/NCP partitioning, with 19–27% of NCP in the plume and 24–26% of NCP in the upwelling zones converted to DOC. A positive correlation was also found between particulate organic carbon (POC) and net DIC consumption, with higher POC production in the upwelling zones where large phytoplankton prevailed. Most NCP removal occurred through POC sinking and/or the diffusion and horizontal transport of DOC.

As one of the largest carbon reservoirs in the ocean, dissolved organic carbon (DOC) is a critically important component of carbon cycling (Hansell and Carlson 2001). Hansell and Carlson (1998) summarize that annual global net DOC production is ~2.0 Pg C yr^{-1}, the magnitude of which is similar to the net ocean-atmosphere CO_2 exchange flux (1.9 Pg C yr^{-1}) (Carlson and Hansell 2015 and references therein). However, characterizing and quantifying the source, production, fate, and bioavailability of marine DOC remains a difficult problem (Hansell 2013). In addition to riverine inputs (Dai et al. 2012), it is generally known that marine DOC is produced by primary producers, frequently observed during phytoplankton blooms, and the modification and fate of DOC are often controlled by microbes (Azam 1998). Due to temporal and spatial decoupling of biological production and removal (Carlson and Hansell 2015 and references therein), net DOC production is always present in the high-latitude regions during the bloom season (Carlson et al. 1994, 2000). Elsewhere in some low-latitude regions, for example, in the Arabian Sea, net DOC production is reported during the period of the Northeast Monsoon (Hansell and Peltzer 1998). Because of higher rates of primary productivity, the coastal ocean is a regime where net production of DOC is frequently observed (Álvarez-Salgado et al. 2001; Dai et al. 2009; Wu et al. 2015).

However, the high degree of interplay among physical, biological, and chemical processes in the coastal ocean makes quantification of net DOC production difficult. Two important processes often shape DOC distribution in the coastal ocean: river plumes and coastal upwelling. The input of organic matter by the river plume increases coastal DOC concentrations, and the upwelling of low-DOC water decreases DOC concentrations. However, nutrients supplied by the river plume and/or coastal upwelling enhance biological production, elevating DOC concentrations.

Low DOC is often observed during the early stages of coastal upwelling events (Doval et al. 1997). Increases in DOC concentrations can be observed following a phytoplankton bloom stimulated by upwelled nutrients, often

*Correspondence: mdai@xmu.edu.cn

downstream of the upwelling circulation (Álvarez-Salgado et al. 1999, 2001). For example, net DOC production of ~37 μmol L^{-1} was measured in the surface water of the Oregon upwelling system (Hill and Wheeler 2002). Similarly, in the coastal upwelling system off the Ria de Vigo (NW Spain), excess DOC production of ~21 μmol L^{-1} was found in the surface water following a phytoplankton bloom (Doval et al. 1997).

The dynamics of DOC in a river plume are additionally complicated due to multiple processes associated with its sources and sinks. Processes contributing to the source of DOC include: the river inputs, phytoplankton production, sediment efflux, particle desorption, and atmospheric deposition (Bauer and Bianchi 2011). DOC can then be removed and/or transformed via microbial and photochemical degradation, as well as particle sorption (Bauer and Bianchi 2011). Net production of DOC is often present in river plumes at mid-high salinity regimes, where photosynthetically active radiation (PAR) favors phytoplankton growth associated with net dissolved inorganic carbon (DIC) consumption (Guo et al. 2009). Examples include many river-dominated systems such as the Mississippi River estuaries, Chesapeake Bay, and the Amazon River plume (Benner and Opsahl 2001; Chen and Gardner 2004; Wang et al. 2004; Meador and Aluwihare 2014). However, net removal of DOC in the river plume is reported on the Eastern Siberian Arctic shelf due to the degradation of terrestrial DOC and limited addition of DOC by marine phytoplankton production (Alling et al. 2010). Therefore, it remains an open question why in some river-dominated plume systems we see net DOC consumption, while in others net production is observed.

Here, we examined the northern South China Sea (NSCS) in the summer, a physically and biogeochemically complex system shaped largely by both a river plume and coastal upwelling. Our focus was DOC and particulate organic carbon (POC) dynamics, including biological production. By adopting a three end-member mixing model, we were able to semiquantitatively estimate the relative rates of net DOC production in the river plume and upwelling zones. Coupled with our parallel examination of nutrients and the carbonate system (Cao et al. 2011; Han et al. 2012), we assessed the carbon partitioning of the net community production (NCP) in the plume and coastal upwelling zones.

Materials and methods

Study area and cruise background

The NSCS shelf in summer is a system under the influence of both a river plume and coastal upwelling. The strong river plume originates from the Pearl River, the 17th largest river in the world in terms of water discharge volume (Dai et al. 2014), with 80% of the discharge during the summer wet season. Coastal upwelling currents occur in both alongshore and cross-shore directions owing to the prevailing southwest monsoon and the highly variable shelf topography (Gan et al. 2009a,b; Han et al. 2012 and references therein). Our cruise to the NSCS shelf on board the *R/V Shiyan* was conducted in summer 2008 within the framework of the South China Sea Coastal Oceanographic Process Experiment (SCOPE) project. The cruise consisted of two legs. During Leg 1 (30 June to 08 July), seven cross-shelf transects covering the major plume-upwelling regions were intensively investigated. Transects 2–5 were repeated during Leg 2 on 09–12 July. An additional station (S401b) was located between Transects 4 and 5 along the inner 30 m isobaths (Fig. 1).

Cao et al. (2011) indicated that continuous heavy rain occurred for about 10 d prior to our cruise. This resulted in the Pearl River discharge peaking at ~43,000 m^3 s^{-1} on 16 June but falling to ~22,000 m^3 s^{-1} on 15 July. Such river discharges were much higher than the annual mean of about 6700 m^3 s^{-1}, or the monthly long-term average of ~14,000 m^3 s^{-1} in wet seasons from June to August (Han et al. 2012).

Sampling and methods

Sample collection

Hydrographic measurements and water sampling were undertaken with a Seabird 911 conductivity-temperature-depth (CTD) unit mounted on a rosette sampling assembly. Samples for DOC were filtered through inline precombusted GF/F filters held in acid-washed polycarbonate filter holders. The filter holder was attached directly to the Niskin bottle with an acid-cleaned and Milli-Q water rinsed silicon tube. Samples were collected in 40 mL precombusted EPA vials, stored at −20°C, and then shipped to the laboratories on land. For POC samples, 4 liter of seawater was filtered through a 25-mm diameter quartz microfiber filter (nominal pore size ~1.0 μm) for further analysis (Zhou et al. 2013).

DOC and POC analysis

All DOC samples were analyzed using a Shimadzu TOC-V/TN system, following the processes described in Wu et al. (2015). Seawater DOC standards, including the low carbon water (1–2 μmol L^{-1}) and deep seawater (41–44 μmol L^{-1}), produced at Hansell's laboratory at the University of Miami, were analyzed to maintain data quality control. Samples were checked against the low carbon and deep reference waters every 5 and 10 sample runs, respectively. The coefficient of variation of replicate measurements was approximately 2%. The standard deviation of deep reference waters throughout our measuring time series was ± 0.8 μmol L^{-1}, which was a useful index of our analytical precision.

All POC samples were placed in Petri dishes and fumed using concentrated hydrochloric acid for 24 h to remove carbonates. Then, POC and particulate organic nitrogen (PON) concentrations were determined using a PE-2400 SERIES II CHNS/O analyzer, following the methods in Zhou et al. (2013). Replicate procedural C and N blanks from sampling

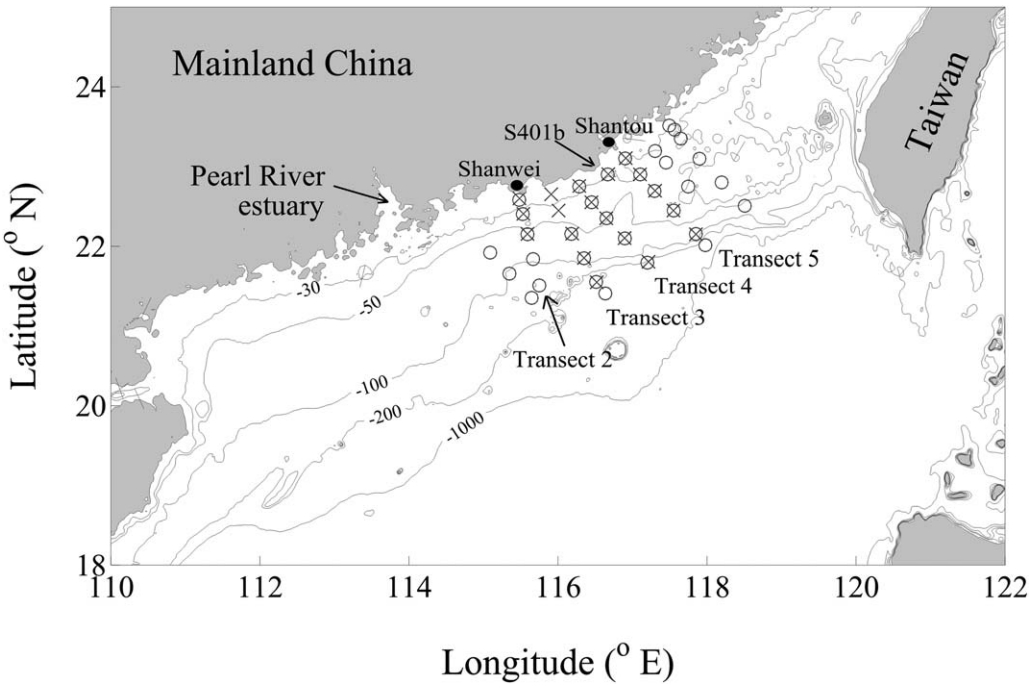

Fig. 1. NSCS topography and sampling stations during June–July, 2008. Circles denote sampling sites during Leg 1 on 30 June to 08 July, and crosses denote those in Leg 2 on 09–12 July.

and instrumental carbon determination were tested by Chen (2008) and Zhou et al. (2013), and were all less than 6 and 2 μg N, respectively, which accounted for less than 10% of the sample POC and PON. The precision of our POC measurements was always <10% (Chen 2008).

Three end-member mixing model

A well-validated three end-member mixing model as introduced in Cao et al. (2011) and Han et al. (2012) was applied to derive conservative concentrations of DOC in this dynamic system influenced by the river plume and upwelling. This three end-member mixing model was based on mass balance equations for potential temperature, salinity, and the water fractions originating from the three end-members as follows:

$$\theta_{RI}F_{RI}+\theta_{SUR}F_{SUR}+\theta_{SUB}F_{SUB}=\theta_{in\ situ} \quad (1)$$

$$S_{RI}F_{RI}+S_{SUR}F_{SUR}+S_{SUB}F_{SUB}=S_{in\ situ} \quad (2)$$

$$F_{RI}+F_{SUR}+F_{SUB}=1 \quad (3)$$

where $\theta_{in\ situ}$ and $S_{in\ situ}$ are the potential temperature and salinity in the water samples; the subscripts RI, SUR, and SUB represent the three different sources: the Pearl River plume, the South China Sea (SCS) surface water, and the subsurface water; and F_{RI}, F_{SUR}, and F_{SUB} are the respective water fractions of the river plume, the SCS surface water, and the subsurface water. The conservative concentrations of DOC (DOC^o) could then be calculated by mixing the three end-members as:

$$DOC^o=DOC_{RI}F_{RI}+DOC_{SUR}F_{SUR}+DOC_{SUB}F_{SUB} \quad (4)$$

where DOC_{RI}, DOC_{SUR}, and DOC_{SUB} are the DOC concentrations of the three end-members. The difference between the conservative and measured DOC concentrations represent the biologically modulated DOC, or ΔDOC (Eq. 5). Positive values indicate net DOC production and negative values suggest net DOC consumption.

$$\Delta DOC=DOC_{in\ situ}-DOC^o \quad (5)$$

The potential temperature and salinity of the three end-members were defined to calculate the water fractions contributed by each. Briefly, the SCS surface water with values of $\theta = 28.6°C \pm 1.0°C$ and $S = \sim 33.7 \pm 0.2$ served as the end-member of the offshore surface water, and the colder SCS subsurface water with values of $\theta = 17.3°C \pm 1.0°C$ (in Leg 1), $\theta = 16.8°C \pm 1.0°C$ (in Leg 2), and $S = 34.6 \pm 0.05$ was used as a proxy of upwelling in the surface waters. We defined the plume water end-member as water with $\theta = 27.0°C \pm 1.0°C$ and $S = 24.5$ using previous measurements off the Pearl River estuary mouth (Gan et al. 2009a).

For the end-member values of DOC in the offshore surface and subsurface waters, we used the average measured DOC concentration of each water mass. In order to better define the end-member value of DOC in the Pearl River plume, we constructed a mixing line of DOC in the Pearl River estuary based on measurements from a later cruise conducted in August 2008. We observed that DOC remained

overall conservative at $S < 24.5$, consistent with the observation that DOC mixes conservatively in the mid-estuary (Callahan et al. 2004; He et al. 2010; Dai et al. 2014). Assuming that the DOC concentration at $S = 0$ during our sampling periods was similar to that in August 2008, we obtained an average DOC concentration at $S = 24.5$ (the plume end-member), of 86 μmol L^{-1}.

Because the dissolved Ca^{2+} is almost conservative in seawater, in spite of small changes resulting from $CaCO^3$ production or dissolution (Cao and Dai 2011), we can use the Ca^{2+} data measured in Leg 1 to evaluate the applicability of our three end-member mixing model. Based on the water fractions derived from Eqs. 1-3 and the end-member values of Ca^{2+}, we calculated the model-predicted Ca^{2+} in the mixing waters. The model predictions and the observations were strongly correlated with a slope of nearly 1 ($y = 0.9992X$, $R^2 = 0.986$, $N = 162$, $p < 0.0001$), suggesting that the three end-member mixing model worked well in predicting the concentrations of Ca^{2+} on the NSCS shelf. This provided direct evidence for the applicability of our three end-member mixing model.

To better quantify the net production rates of DOC in the plume and upwelling regions, the uncertainties derived from the three end-member mixing model need to be further constrained. Based on Eqs. 1–5, the sources of uncertainty in the derivation of ΔDOC values were associated with the uncertainties of potential temperature, salinity, and the DOC concentrations of the three end-members.

Similar to Han et al. (2012), we used the deviations of DOC in the surface and subsurface end-members, i.e., 2 and 1.5 μmol L^{-1}, as the uncertainties of DOC. We based the DOC variability in the river plume end-member (at $S = 24.5$) on the August 2008 cruise data from the Pearl River estuary, assigning a value of 3 μmol L^{-1}.

We then calculated the corresponding uncertainties of average net DOC production induced by the variations of potential temperature, salinity, and DOC in the end-members as ~0.6 μmol L^{-1}, which was much smaller than the standard deviations of average ΔDOC values in the plume (5.6 μmol L^{-1}) and upwelling zones (4.1 μmol L^{-1}). Other DOC sources such as rainfall may also add additional uncertainty to our estimations. Based on the reported regional precipitation rates and typical rainwater DOC concentrations (Jurado et al. 2008; Li et al. 2010; Li et al. 2013), we found that the precipitation fluxes of DOC and DIC on the NSCS shelf are very small, accounting for 1.5–8.7% (average = 4.2%) of DOC production and 0.7% of DIC consumption. Most importantly, considering the mixed-layer depth and the average residence time in the plume and upwelling regions, these atmospheric input fluxes of DOC (0.31 μmol L^{-1} in the plume and 0.46 μmol L^{-1} in the upwelling zones) are well within the range of uncertainty (0.6 μmol L^{-1}) in our study and are much smaller than the standard deviation of average ΔDOC values. Thus, we concluded that the estimation of net DOC production using our model was reasonable.

Results

Hydrography

Cao et al. (2011) and Han et al. (2012) describe the basic hydrology of the NSCS shelf measured during the cruise (Legs 1 and 2). Briefly, the hydrological characteristics of the study area were highly controlled by a strong river plume and coastal upwelling. This was further reflected in the T-S diagram (Fig. 2), which showed that the water masses in our study area were mainly a mixture of the river plume, the SCS surface water, and the SCS subsurface water. In general, patches of plume water spread eastward across the NSCS shelf. During Leg 1, two low-salinity centers were found, one on the inner shelf between Transects 1 and 2 and the other on the middle shelf at Transect 5. These plume centers disappeared during Leg 2 as a result of the weakened riverine discharge (Fig. 3). Low-temperature (22.8–26.0°C) and high-salinity (33.9–34.3) waters similar to the SCS subsurface end-member outcropped on the inner shelf with the center located in the nearshore water between Transects 4 and 5 (Fig. 3) during Leg 1. However, the coastal upwelling water occupied a much smaller area during Leg 2.

The temperature and salinity distribution along Transect 2 indicates that cold deep water upwelled along the slope and toward the shore during Legs 1 and 2 (Fig. 4). Water outcropping nearshore along Transect 2 was colder during Leg 2 than during Leg 1, suggesting stronger upwelling intensity. Surface salinity (Fig. 3) was higher in Leg 2, suggesting the weakened input of river plume water. Transect 5 was characterized by warm, freshwater in the upper water column, although saline upwelled water is apparent nearshore during both legs and less influence by the plume is evident during Leg 2. The alongshore extension of the river plume tended to inhibit nearshore outcropping of the cold water, which originated near Transect 2 where the strongest upslope cold water advection was located according to Gan et al. (2009a).

Distribution of DOC and POC

The distribution of DOC was also modulated by the mixing of water masses sourced from the plume, upwelled subsurface water, and offshore surface water. In general and as shown in Fig. 2, DOC concentrations were highest in the plume, with relative decreases in the offshore surface and subsurface waters. Additionally, enhanced biological production due to the large nutrient supply from the river plume and subsurface upwelling (Gan et al. 2010) would also influence the distribution of DOC on the NSCS shelf. The biogeochemical controls on the distribution of DOC on the NSCS shelf are presented in detail for surface and vertical distribution of DOC and POC in the sections below.

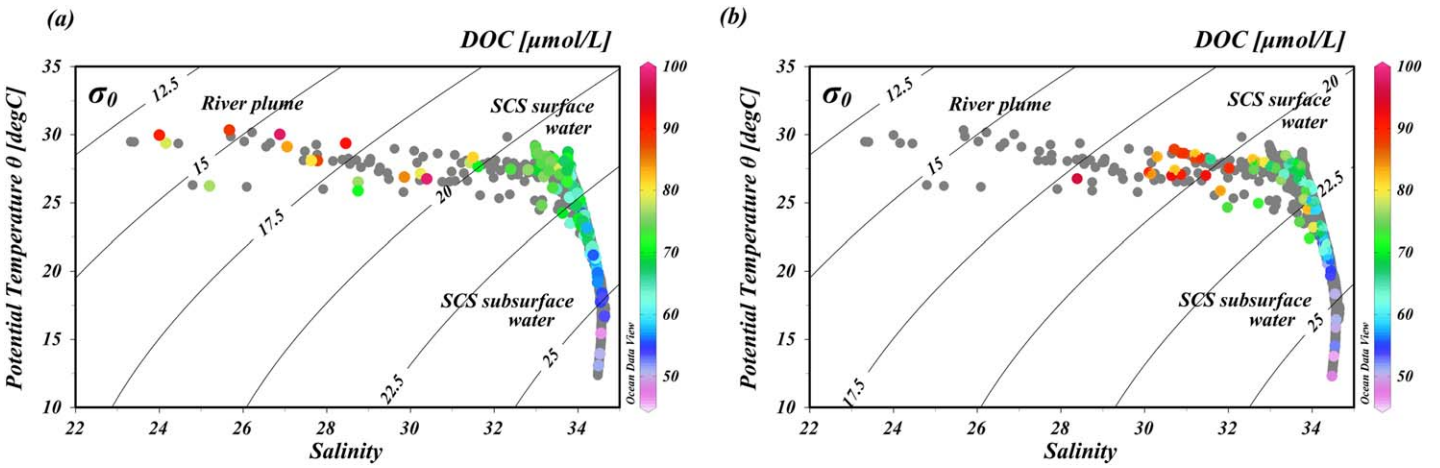

Fig. 2. Potential temperature vs. salinity on the NSCS shelf in summer 2008, superimposed by DOC concentrations during Legs 1 (**a**) and 2 (**b**). Data were collected from a CTD recorder with 1-m resolution throughout the whole water column. The T and S data are shown in Shu et al. (2011) and Han et al. (2012).

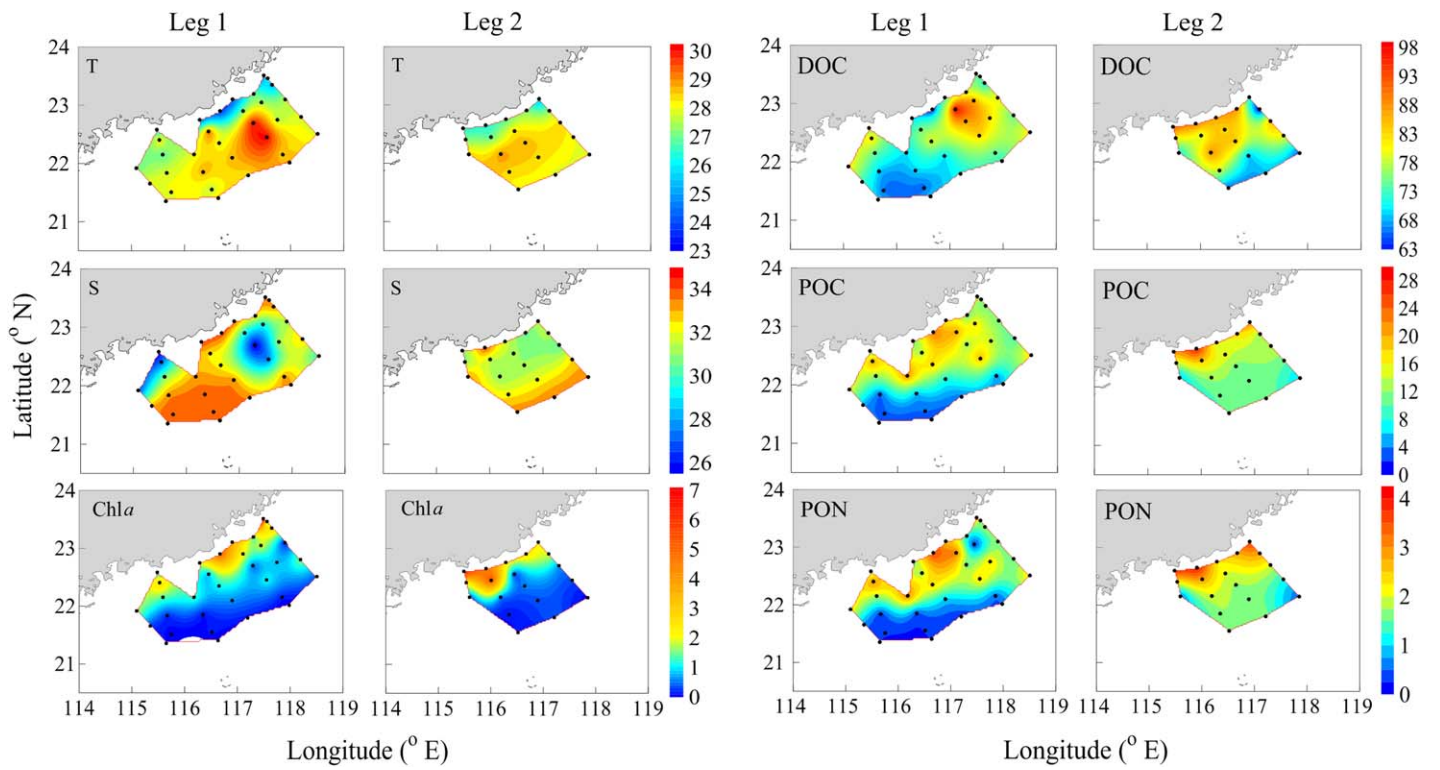

Fig. 3. Surface distribution of temperature (T), salinity (S), Chl *a* (μg L^{-1}), DOC (μmol L^{-1}), POC (μmol L^{-1}), and PON (μmol L^{-1}) on the NSCS shelf during Legs 1 and 2. Surface T, S, and Chl *a* data are shown in Cao et al. (2011) and Han et al. (2012).

Surface distribution

DOC distribution patterns over the shelf reflected the coinfluence of the river plume and coastal upwelling (Fig. 3). Within the plume water, DOC concentrations were significantly elevated, ranging from 70 to 98 μmol L^{-1}. There were no obvious differences in the DOC concentrations of plume water between the two legs. The surface regions occupied by upwelled waters had low DOC concentrations (~63 μmol L^{-1}), even lower than those in the outer shelf surface water of the NSCS, as subsurface waters are characterized by the lowest DOC concentrations. Note that during Leg 2, relatively higher DOC concentrations (~76

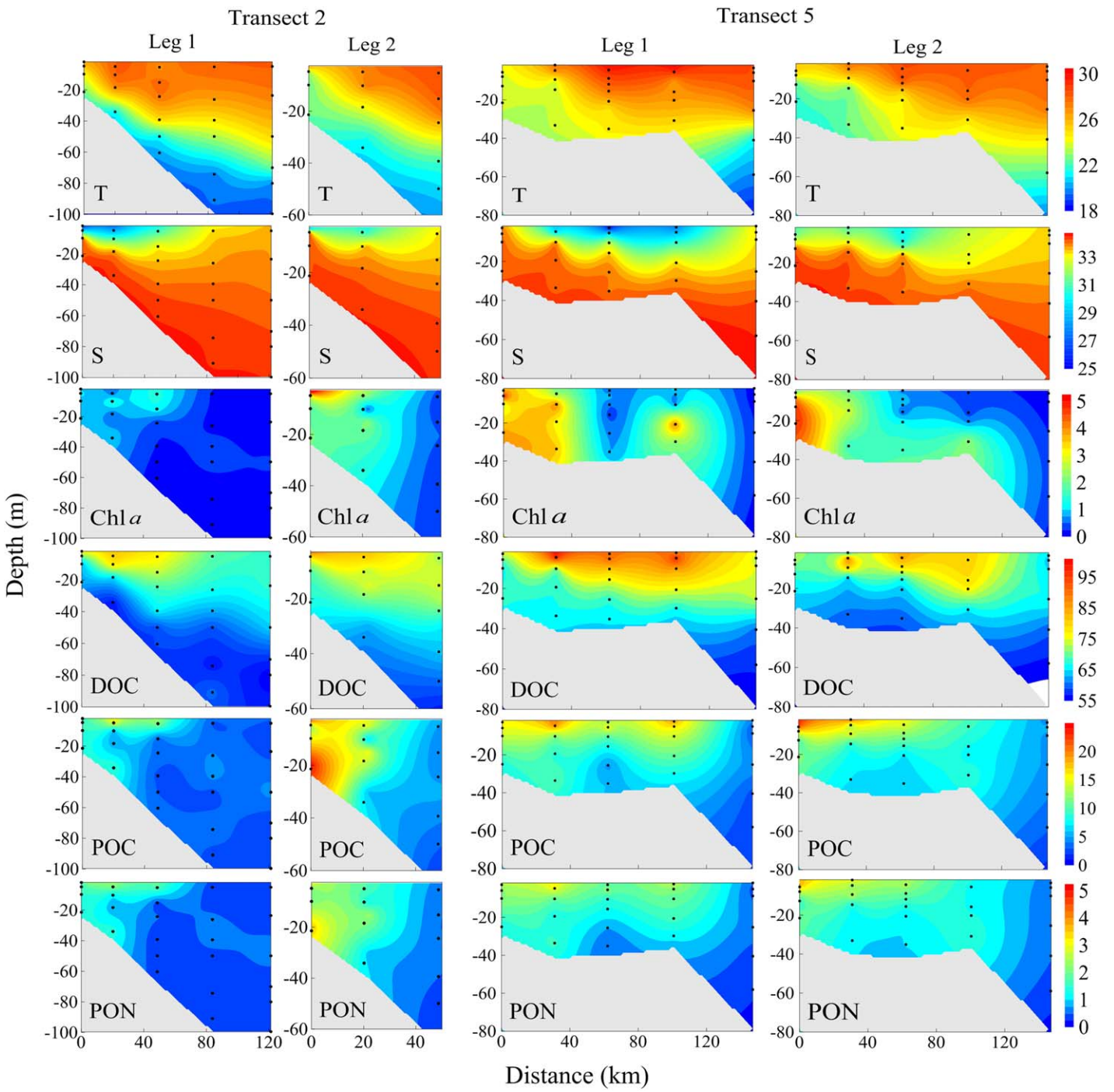

Fig. 4. Vertical distribution of temperature (T), salinity (S), Chl *a* (μg L^{-1}), DOC (μmol L^{-1}), POC (μmol L^{-1}), and PON (μmol L^{-1}) along Transects 2 and 5 on the NSCS shelf during Legs 1 and 2 in summer 2008. T, S, and Chl *a* data are shown in Cao et al. (2011) and Han et al. (2012).

μmol L^{-1}) were measured in the coastal upwelled waters of Transects 2 and 4 than were measured during Leg 1 ($\sim$68 μmol L^{-1}).

Surface POC and PON showed similar patterns on the NSCS shelf with high values in zones influenced by the river plume and upwelling. POC and PON were in the range 2.8–22.1 and 4.6–27.8 and 0.3–3.6 and 0.5–4.6 μmol L^{-1} in Legs 1 and 2, respectively. During Leg 1, POC and PON concentrations in the plume and upwelling were comparable. However, POC and PON concentrations in the upwelling zones during Leg 2 (14.0–27.8 and 2.3–4.0) were relatively higher than those observed during Leg 1 (10.5–22.1 and 1.5–3.6),

suggesting enhanced POC and PON production during Leg 2 due to greater primary production caused by additional nutrients being upwelled from the subsurface water.

Vertical distribution

Vertical distributions of DOC, POC, and PON along Transects 2 and 5 during Legs 1 and 2 are shown in Fig. 4. The surface DOC inversely correlated with salinity. Along Transect 2, values of surface DOC ranged from 76 to 87 μmol L^{-1} during Leg 1, but increased to 82–92 μmol L^{-1} in Leg 2. Surface chlorophyll *a* (Chl *a*), POC, and PON concentrations along Transect 2 also increased from ~2.7 to ~6.6, ~19.8 to ~21.7, and ~2.2 to ~3 μmol L^{-1}, respectively, suggesting elevated biological production of organic matter during Leg 2. Along Transect 5, however, surface DOC concentrations ranged from 81 to 98 μmol L^{-1} during Leg 1, but decreased to 71–88 μmol L^{-1} during Leg 2. Note that during Leg 1, the plume center occupied the middle shelf along Transect 5, owing to the eastward transport of the river plume, and contained higher DOC and POC concentrations than within the plume along Transect 2, suggesting DOC and POC production during the course of plume water transport.

A strong onshore DOC gradient is apparent beneath the plume water along Transect 2, owing to the cold and DOC-depleted water ($DOC < 56$ μmol L^{-1}) at 150 m depth on the slope. Compared to Leg 1, DOC, POC, and PON concentrations increased from ~59 to ~67, ~9.1 to ~24.0, and ~1.5 to ~3.5 μmol L^{-1}, respectively, on the inner shelf along Transect 2 during Leg 2, suggesting enhanced DOC, POC, and PON production. This is supported by the fact that along Transect 2, Chl *a* also increased from ~1.2 μg L^{-1}during Leg 1 to ~2.9 μg L^{-1} during Leg 2. However, on the inner shelf along Transect 5, DOC concentrations were lower during Leg 2 than Leg 1, which is consistent with the observation that nutrient concentrations along Transect 5 were higher during Leg 2 than Leg 1 as a result of the intensified upwelling rather than advection of high DOC plume water to the region. Note that Chl *a*, POC, and PON displayed a subsurface maximum layer in Transect 2, suggesting that both PAR and nutrients in the subsurface layer were available for the growth of phytoplankton.

Discussion

Both surface and vertical distributions of DOC suggested that the dynamics of DOC were influenced mainly by the river plume and upwelling on the northern SCS shelf during the summer. In addition to this physical control, the biological alteration of DOC was apparent in the plume and upwelling zones. Moreover, Cao et al. (2011) and Han et al. (2012) observed the significant net removal of DIC and nutrients in the river plume and upwelling zones, suggesting that the plume and upwelling systems are generally autotrophic. In order to differentiate the extent that DOC distributions are controlled by physical mixing vs. biologically modulated

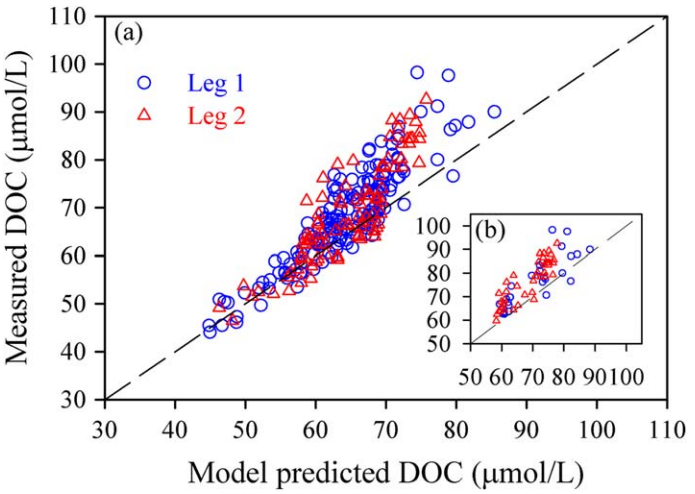

Fig. 5. Measured DOC vs. the predicted DOC derived from the three end-member mixing model in all the stations (**a**) and Transects 2–5 (**b**) during Legs 1 and 2.

DOC production in this plume-upwelling system, we adopted a three end-member mixing model that was also used for carbonate (Cao et al. 2011) and nutrient systems (Han et al. 2012) during the same cruise. To draw comparisons with previous studies, and between Legs 1 and 2, model results from Transects 2–5, which were visited during both Legs, are discussed in detail below.

Net DOC production derived from the three end-member mixing model

A comparison between the field measured and the model predicted DOC is shown in Fig. 5. At $DOC < 60$ μmol L^{-1}, the model predictions agreed well with the field measurements (Fig. 5a), confirming the utility of the model. However, it was clear that most predicted DOC values were lower than the field measurements at $DOC > 60$ μmol L^{-1} during both legs, indicating additional DOC sources, most likely from biological production. In Transects 2–5 (Fig. 5b), a constant offset was found between the field measured and modeled DOC during Legs 1 and 2, suggesting that DOC production was comparable between Legs 1 and 2. Based on the difference (ΔDOC) between the predicted and measured values, the net production of DOC in Transects 2–5 during Legs 1 and 2 was quantified.

According to Gan et al. (2010), the plume water is defined as water with salinity < 33.0 on the shelf. The ΔDOC values in the plume therefore ranged from −5 to 22 and −1.6 to 16 μmol L^{-1} in Legs 1 and 2 (Fig. 6a). The majority of ΔDOC values were positive, suggesting significant biological production of DOC in the river plume. As salinity increased, the ΔDOC values became higher on the NSCS shelf, suggesting the enhancement of net DOC production during the transport of plume water on the shelf. Although the plume area appeared to be reduced during Leg 2 when the river

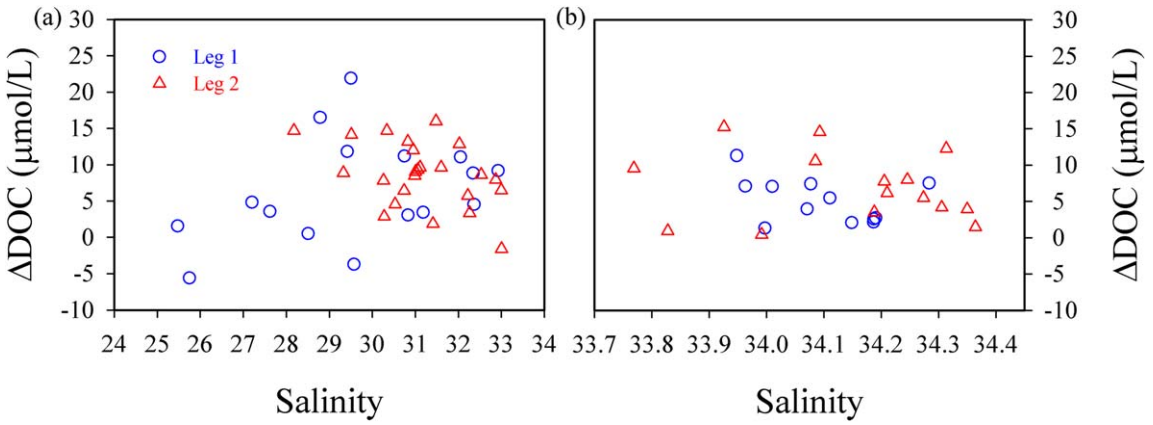

Fig. 6. ΔDOC vs. salinity for the plume water (**a**) and the upwelling water (**b**) in Transects 2–5 on the NSCS shelf during Legs 1 and 2 in summer 2008.

discharge became weakened, the average ΔDOC values displayed no significant difference ($p = 0.198$), with values of 6.7 ± 6.6 μmol L^{-1} during Leg 1 and 8.6 ± 4.6 μmol L^{-1} during Leg 2. The average ΔDOC in the plume (both Leg 1 and Leg 2) was 7.7 ± 5.6 μmol L^{-1}, comparable to the total organic carbon (TOC) production (19 ± 13 μmol L^{-1}) in the Amazon River plume within the margin of error (Meador and Aluwihare 2014). Together with an assumed mixed-layer depth of ~13 m (Cao et al. 2011) and an average residence time of 12.3 d for the river plume during Leg 1 (Liu et al. 2012), we estimated a net DOC production rate of 7.1 ± 7.0 mmol C m^{-2} d^{-1} during Leg 1.

The behavior of DOC in the Pearl River estuary has been previously studied (e.g., Callahan et al. 2004; He et al. 2010). In the upper reaches of the Pearl River estuary, the net removal of DOC is observed, which is consistent with the decrease in DOC biodegradation rates from the head to the mouth of the estuary (He et al. 2010). In the lower mid-high salinity regimes of the Pearl River estuary, DOC behavior is conservative, suggesting that heterotrophic removal of DOC is weak and balanced by autotrophic production (He et al. 2010). Our observations (unpubl.) in the Pearl River estuary prior to the SCOPE cruise conducted on the NSCS shelf confirmed the relatively conservative mixing of DOC in the lower Pearl River estuary, suggesting a balance of DOC production and removal therein. In this study, due to the high river discharge, the river plume extended to the NSCS shelf from the Pearl River estuary. In contrast to the Eastern Siberian Arctic shelf where the net removal of DOC is caused by the degradation of terrestrial DOC with low additions of DOC from marine phytoplankton production (Alling et al. 2010), the elevated Chl *a* concentration and primary production data in the present river plume on the NSCS shelf suggested significant primary productivity associated organic carbon production (Han et al. 2012). Indeed, our results confirmed significant net DOC production as the river plume was transported along the shelf. Similarly, Meador and Aluwihare (2014) observed high nutrient concentrations and primary production rates in the Amazon River plume, accompanied by net DOC production and DIC consumption during its transport to the Atlantic Ocean. It appears that in river-dominated systems where biological production is stimulated, net production of DOC is often observed. Indeed, many river-dominated systems of this nature tend to be net autotrophic, producing organic carbon and acting as strong sinks of atmospheric CO2 (Gattuso et al. 1998; Wollast 1998; Bauer et al. 2013; Guo et al. 2015).

According to Gan et al. (2010), upwelled water on the NSCS shelf is defined as having salinity > 33.75 in the nearshore upper 20 m. All of the ΔDOC values in these regions during the two legs were positive, indicating net DOC production in upwelled subsurface water (Fig. 6b). Most of the ΔDOC values were distributed between 1.3 and 11.3 μmol L^{-1} during Leg 1, and 0.4 and 15.2 μmol L^{-1} during Leg 2. Within the margin of error, the average ΔDOC value in Leg 1 (5.0 ± 3.0 μmol L^{-1}) was comparable to that in Leg 2 (6.9 ± 4.8 μmol L^{-1}). However, average ΔDOC values in Transect 2 and at Sta. S401b (the upwelling center) during Leg 2 were 10 ± 3.6 μmol L^{-1}, which was much higher than those (2.7 ± 0.6 μmol L^{-1}) in Leg 1. This suggested that net DOC production was enhanced when the upwelling was strengthened and outcropped during Leg 2. Assuming a mixed-layer depth of ~20 m and a residence time of ~8.7 d on the nearshore shelf during Leg 1 (Liu et al. 2012), the net DOC production rate in the upwelling zone was estimated as 11.5 ± 6.9 mmol C m^{-2} d^{-1}. Although Cao et al. (2011) and Han et al. (2012) estimate that NCP in the plume is slightly higher than or comparable to that in the upwelling zone, and Gan et al. (2010) also simulate relatively lower surface primary productivity in upwelled waters relative to the plume, the average net DOC production rate (7.1 ± 7.0 mmol C m^{-2} d^{-1}) for the plume water was comparable to the upwelled water mass (11.5 ± 6.9 mmol C m^{-2} d^{-1}) within the margin of error.

Many factors influence the production and bioavailability of DOC during coastal upwelling (Doval et al. 1997; Lønborg et al. 2010; Halewood et al. 2012; Wear et al. 2015). For example, the extracellular release (ER) of DOC by phytoplankton may differ over upwelling stages, with low ER values during the intensified upwelling period, and relatively high ER values under lower nutrients concentrations over the relaxed upwelling period (Carlson et al. 1998; Wetz and Wheeler 2003). This would result in relatively high DOC productivity when nutrient concentrations are low in the upwelling zone. Correspondingly, the elementary stoichiometry, molecular size, and composition of DOC may differ over these upwelling stages, and in combination with nutrient concentrations will also influence the bioavailability of DOC (Williams 1995; Halewood et al. 2012). Halewood et al. (2012) report the relatively high bioavailable DOC fractions during upwelling, and lower fractions during the transition of upwelling to back to stratified conditions. In this study, during the intensified upwelling period, the positive correlations (not shown) between net DOC production and Chl *a* suggested that the accumulated DOC was mainly contributed by the phytoplankton. The DOC released from phytoplankton is readily bioavailable and can be quickly utilized by the bacteria (Shen et al. 2012). Given the ΔDOC and the field measured DOC, we estimated that the bioavailable fraction of DOC could account for 10% ± 5% of the total DOC pool in the upwelling zone, which was comparable with previous results (17% ± 6% and 9–18%) reported in the upwelling systems of the Ria de Vigo (NW Iberian Peninsula) and Santa Barbara Channel (Lønborg et al. 2010; Halewood et al. 2012).

Han et al. (2012) reported that DIC and nutrients are regenerated during the alongshore advection of subsurface water to Shanwei (Fig. 1), observing a northward increasing trend of DIC and dissolved inorganic nitrogen (DIN) (nitrate + nitrite) consumption along the upwelling coastal current from Shanwei (Transect 2) to Shantou (Transect 5) (Fig. 1). For further discussion of the coupling of DOC production with DIC and DIN consumption on the NSCS shelf, the distributions of ΔDOC, ΔDIC and ΔDIN along Transects 2 and 5 are presented in Fig. 7. Here, ΔDIC and ΔDIN denote the differences in DIC and DIN between model predictions and the field measured values. Positive values reflect net consumptions of DIC and DIN.

As expected, most of the ΔDOC, ΔDIC, and ΔDIN values along Transects 2 and 5 were positive, especially in the plume of Transects 2 and 5, suggesting the coupling of DOC production with the consumption of DIC and DIN. Interestingly, it should be noted that positive ΔDOC values and negative ΔDIC and ΔDIN values were found in the cross-shelf upwelling water of Transect 2, linking DOC production to the addition/regeneration of DIC and DIN. Previous studies demonstrate that the decomposition of POM results in the regeneration of DIC and DIN in upwelled water masses (Cao et al. 2011; Han et al. 2012). During this decomposition, some POM can be transformed to dissolved organic matter (DOM) via bacterial hydrolysis (Smith et al. 1992). In addition, regenerated nutrients in the upwelling zone, when transported to nearshore areas, could stimulate the growth of phytoplankton and organic carbon production.

The comparisons of ΔDOC, ΔDIC, and ΔDIN between Transects 2 and 5 reflected the biological alteration of DOC, DIC, and DIN during the transport of the plume and the upwelled water mass. Consistent with the increase of ΔDIC and ΔDIN in the plume from Transect 2 to Transect 5, ΔDOC was also higher in Transect 5 than in Transect 2, indicating the enhancement of DOC production during plume transport. Similarly, along with the northward consumption of DIC and DIN along the inner shelf during the transport of upwelled water from Shanwei (Transect 2) to Shantou (Transect 5), DOC production was also enhanced during Leg 1. However, during Leg 2, ΔDOC in the inner shelf of Transect 2 was higher than in Transect 5, suggesting the decomposition of accumulated DOC during the northward transport of upwelled water, which also explained the regeneration of nutrients observed by Han et al. (2012).

Carbon partitioning of NCP in the plume and upwelling zones

DOC

Assuming that the uptake ratio of DIC: DIN: dissolved inorganic phosphate (DIP) by the phytoplankton followed the Redfield ratio (106 : 16 : 1), the NCP is equivalent to ΔDIC, 6.6ΔDIN, or 106ΔDIP. In order to quantify the fractions of the NCP transformed to DOC, ΔDOC was plotted with ΔDIC, 6.6ΔDIN, and 106ΔDIP in the plume and upwelling zones. As shown in Fig. 8a–c, significant correlations were observed between ΔDOC and ΔDIC, 6.6ΔDIN and 106ΔDIP in the plume during Legs 1 and 2, indicating the coupling of net DOC production with the net consumption of DIC, DIN, and DIP in the plume, which was consistent with the previous observation (Meador and Aluwihare 2014) that DOC production increases linearly with the enhanced consumption of DIC in the Amazon River plume. The slopes of the linear regressions of ΔDOC vs. ΔDIC, 6.6ΔDIN, and 106ΔDIP in the plume were comparable between Legs 1 and 2, in the range of 0.19–0.26, 0.26–0.27, and 0.49–0.82, respectively. The slopes of ΔDOC vs. ΔDIC were close to that of ΔDOC vs. 6.6ΔDIN, confirming that 19–27% of the NCP was converted to DOC in the plume water. However, the slopes of ΔDOC vs. 106ΔDIP (0.49–0.82) were much higher than those of ΔDOC vs. ΔDIC and 6.6ΔDIN. Indeed, Han et al. (2012) also find apparent non-Redfield uptake ratios (> 16 : 1) of DIN : DIP in the river plume, likely due to the quick decomposition of DOP (dissolved organic phosphorus). Thus, the NCP or organic production in the river plume estimated based on the net consumption of DIP would be subject to large uncertainty.

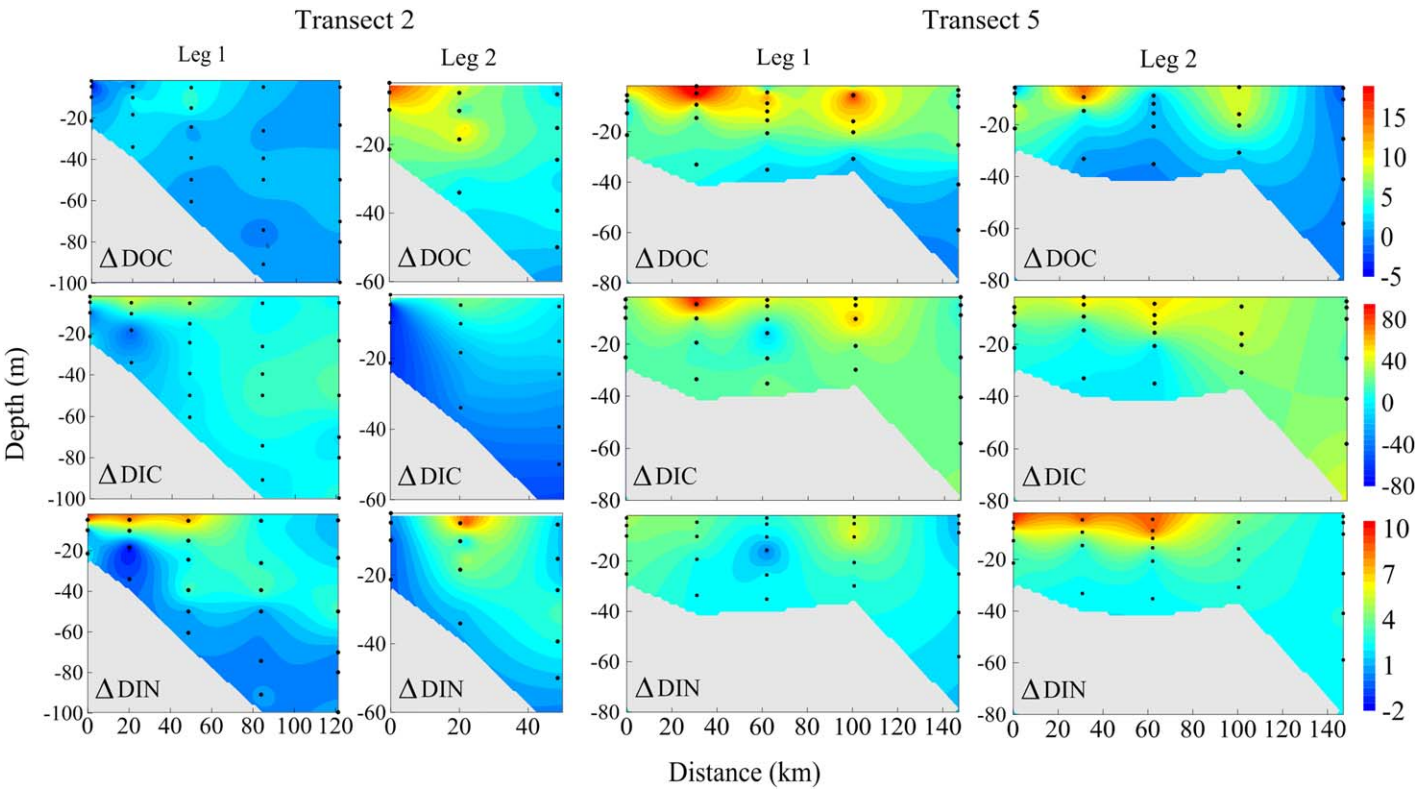

Fig. 7. Distributions of ΔDOC (μmol L^{-1}), ΔDIC (μmol L^{-1}), and ΔDIN (μmol L^{-1}) along Transects 2 and 5 on the northern SCS shelf in summer 2008 during Legs 1 and 2. ΔDIC, ΔDIN, and ΔDIP, representing the biological alterations of DIC, DIN, and DIP on the northern SCS shelf, are the differences between measured and model predicted concentrations, as estimated by Cao et al. (2011) and Han et al. (2012). Positive values of ΔDIC, ΔDIN, and ΔDIP indicate net consumption, while the negative values suggest net production/addition.

In the upwelling zones, significant correlations between ΔDOC and ΔDIC and 6.6ΔDIN and 106ΔDIP were found only during Leg 1 (Fig. 8d–f). This was because most of the ΔDIC values observed during Leg 2 were negative, due to the DIC addition caused by the remineralization of POM in the near-bottom onshore-flowing water (Cao et al. 2011). However, the trend of higher ΔDOC values as ΔDIC decreased was still apparent during Leg 2, suggesting that DOC production was enhanced as the regenerated nutrients and DIC were transported to the inner shelf and stimulated primary production. The slopes of ΔDOC vs. ΔDIC and 6.6ΔDIN and 106ΔDIP in the upwelling zone during Leg 1 were relatively constant as 0.24, 0.25, and 0.26, suggesting that 24–26% of the NCP was converted to DOC in this region. Similar carbon partitioning of NCP is also observed in the Ria de Vigo upwelling system (Iberian margin of the North Atlantic), where DOC production accounts for 20% of net primary production (Álvarez-Salgado et al. 2001). Note that although primary production and the phytoplankton community structure (W. Lei unpubl.) in the plume and upwelling zones were different, the fractions of NCP accumulated as DOC in the river plume and upwelled water masses were comparable. Our study supported the notion that DOC production accounts for approximately 20% of NCP in the coastal ocean (Hansell and Carlson 1998).

Suspended POC

The similar distribution of POC and Chl *a* suggested biological production of POC while the phytoplankton bloomed in the plume and upwelled water. Moreover, the slopes of POC/PON in the plume (6.3 ± 0.6) and upwelled water (6.4 ± 0.9) were consistent with the Redfield ratio, further confirming the marine source of POM. The POC/Chl *a* ratio in the coastal ocean is often used to distinguish freshly produced POM (Liu et al. 2007; Cai et al. 2012). The freshly produced POM has a POC/Chl *a* ratio lower than 200 (Cifuentes et al. 1988; Liu et al. 2007). In the plume, POC/Chl *a* was in the range 47.3–326.4 and 24.3–380 with averages close to 200 (175.7 ± 86.2 and 165.3 ± 116.4 during Legs 1 and 2, respectively), indicating that POC in the plume was contributed mainly by biogenic particles such as detritus, bacteria and viruses. However, POC/Chl *a* values in the upwelling zones were lower than 200 with averages of 54.8 ± 38.7 and 71.2 ± 52.3, respectively, suggesting that phytoplankton carbon dominated POC in upwelled subsurface water.

As shown in Fig. 9, positive linear correlations were observed between POC and ΔDIC in the plume during both legs and in the upwelling zone during Leg 1, suggesting that the POC production was associated with the net consumption of DIC. Similar to ΔDOC, the negative correlation

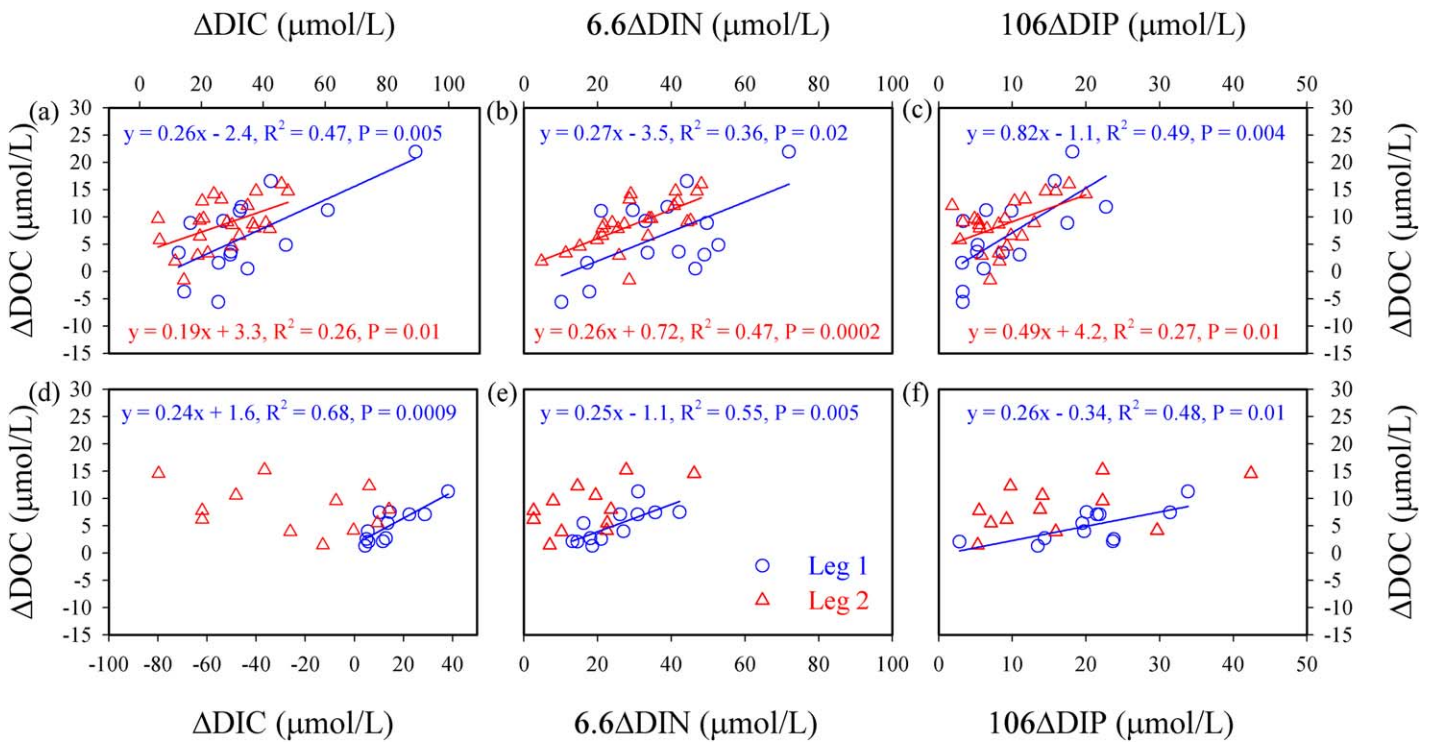

Fig. 8. ΔDOC vs. ΔDIC (**a, d**), 6.6ΔDIN (**b, e**), and 106ΔDIP (**c, f**) in the plume (**a–c**) and upwelling (**d–f**) on the NSCS shelf in summer 2008 during Legs 1 and 2.

between POC and ΔDIC confirmed enhanced organic matter production while the regenerated DIN/DIC in the upwelled subsurface water was transported to the inner shelf, stimulating primary production. The intercepts of the linear regression lines (8.3 and 8.6 μmol L^{-1} in the plume during Legs 1 and 2, and 7.7 μmol L^{-1} in the upwelling zone during Leg 1) represented the initial POC concentrations in the plume and upwelled water prior to the net DIC consumption. Therefore, the net biological production of POC (ΔPOC) in the plume and upwelled water, due to the net consumption of DIC, could be roughly estimated as the subtraction between the field measured POC and the $POC_{\Delta DIC=0}$. Accordingly, we could estimate that the ΔPOC was in the range −3.0 to 11.2 μmol L^{-1} during Leg 1 and −1.0 to 13.5 μmol L^{-1} during Leg 2 in the plume, and −1.3 to 7.8 μmol L^{-1} during Leg 1 in the upwelling zone. The high POC production (up to 11.2–13.5 μmol L^{-1}) is present in the plume and upwelling zones with high NCP. The slopes of POC vs ΔDIC (0.14–0.18 in the plume and 0.27 in the upwelling zone) indicated that POC production accounted for 14–18% and 27% of the NCP, respectively, in the plume and upwelling zone. Furthermore, we estimated that the net TOC production (ΔTOC = ΔDOC + ΔPOC) was in the range −4.7 to 33.0 μmol L^{-1} during Leg 1 and 0.3–28.2 μmol L^{-1} during Leg 2 in the plume, and 0.8–20.4 μmol L^{-1} during Leg 1 in the upwelling zone. The average values of ΔPOC and ΔTOC in the plume (4.8 ± 2.8 and 11.4 ± 9.5 μmol L^{-1} in Leg 1; 5.0 ± 2.1 and 14.0 ± 5.3 μmol L^{-1} in Leg 2) were comparable to those (4.0 ± 2.8 and 8.9 ± 5.6 μmol L^{-1}) in the upwelling zone. Given the residence times of plume and upwelling waters on the NSCS shelf during Leg 1, we estimated that the net POC production rates in the plume and upwelling zone were 5.1 ± 3.0 and 9.2 ± 6.4 mmol C m^{-2} d^{-1}, and the net TOC production rates were 12.1 ± 10.1 and 20.5 ± 12.9 mmol C m^{-2} d^{-1}.

Although ΔPOC and ΔTOC were comparable between the plume and the upwelling zones within their uncertainties, the partitioning of TOC production displayed different patterns. As shown in Fig. 9c,d, the slopes of ΔPOC vs. ΔTOC in the plume (0.32–0.46) and upwelling zones (0.58) indicated that POC production accounted for 32–46% of TOC production in the plume, and 58% in the upwelled water. DOC production dominated the TOC production in the plume, while it was less than POC production in the upwelling zones. The relatively high POC production in the upwelled water was consistent with reports in other upwelling systems (Wetz and Wheeler 2003; Halewood et al. 2012). Previous studies suggest that organic carbon production partitioning during a phytoplankton bloom is correlated with the community structure and food web dynamics (Carlson et al. 1998, Lomas and Bates, 2004). Organic carbon is partitioned mainly into POC when diatoms dominate the biomass during a phytoplankton bloom (Engel et al. 2002; Wetz and Wheeler 2003), and into DOC when the picoplankton dominate (Casareto

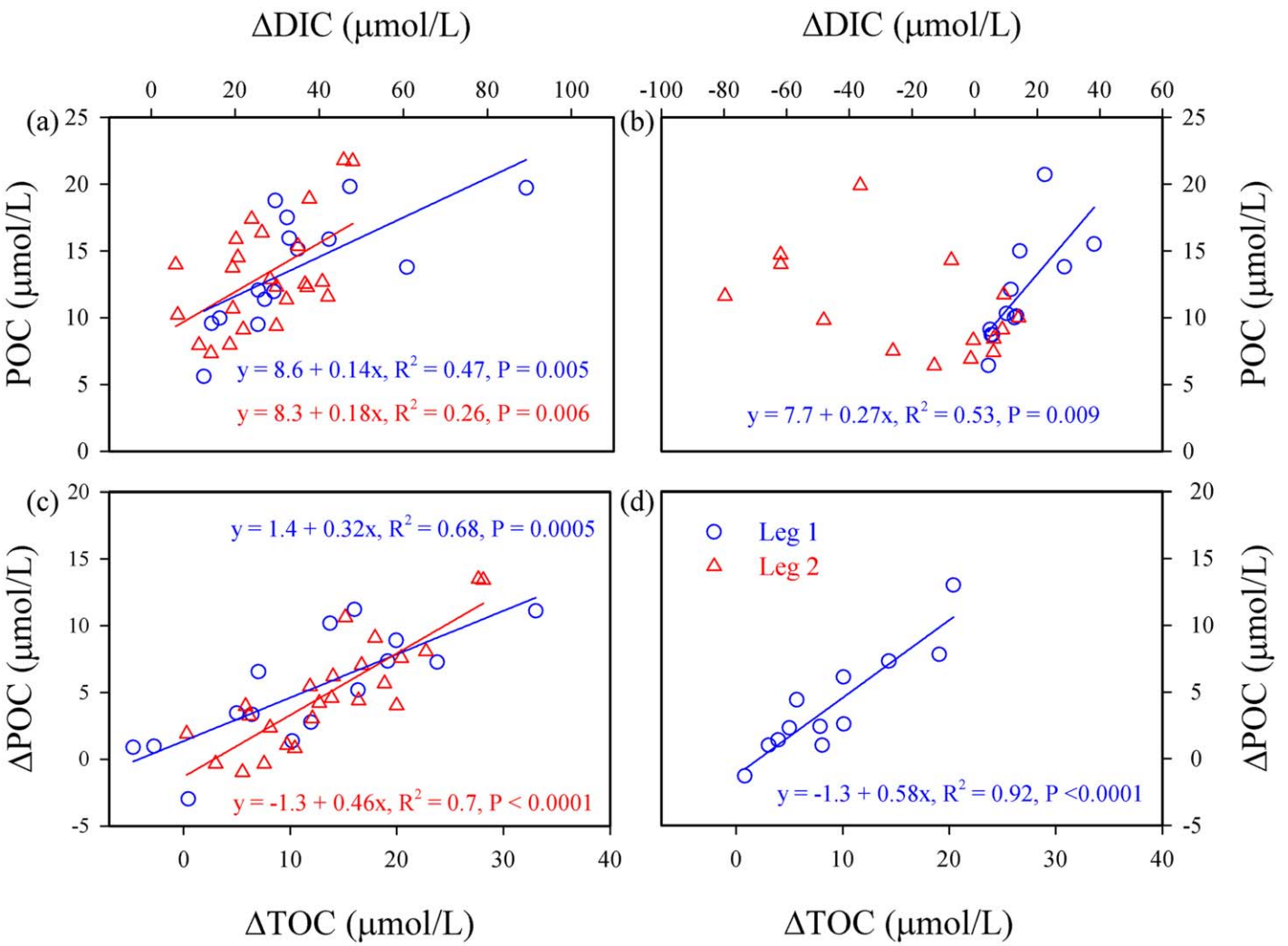

Fig. 9. POC (**a, b**) vs. ΔDIC and ΔPOC (**c, d**) vs. ΔTOC in the plume (**a, c**) and upwelling (**b, d**) during Leg 1 (blue dots) and Leg 2 (red triangles). ΔPOC and ΔTOC denote the net POC and TOC (POC + DOC) production.

et al. 2012 and references therein). The phytoplankton community structure data derived from the same cruise (W. Lei unpubl.) showed that diatoms dominated in the phytoplankton biomass of the upwelling zone, which may have caused the relatively high POC production in this water mass during our study.

Biogeochemical implications

Owing to the abundant nutrients carried by the Pearl River plume (Dai et al. 2008a,b; Han et al. 2012; Dai et al. 2014) and coastal upwelling (Gan et al. 2010; Han et al. 2012), the phytoplankton bloom resulted in significant consumption of DIC and DIN, and the production of organic carbon on the NSCS shelf during summer. Apart from the organic carbon accumulated in the water column, the fate of the NCP in the plume and upwelled water massed included organic carbon being removed from the water column through the sinking of the POM, the diffusion and turbulent mixing of DOC, and/or the horizontal transport due to advection. The partitioning of organic carbon produced in the coastal ocean can have important implications for the fate of NCP by affecting the carbon transport pathways (Wetz and Wheeler 2003).

Chen (2003) reports that at least 4% of the global net primary production of the coastal ocean is exported to the adjacent open ocean as DOC, which accounts for at least 15% of the DOC accumulated in the surface layer of the global ocean (Lønborg and Álvarez-Salgado 2012 and references therein). In the coastal upwelling system off Iberia and NW Africa, the export of DOC induced by upwelling accounts for ~58% of the generated NCP (Álvarez-Salgado et al. 2007). Our results showed that similar fractions (~27%) of the NCP were transformed to DOC, in spite of the different phytoplankton community structures between the plume and upwelling zones. However, some studies show that DOC

production represents a major fraction of the NCP when nutrients are depleted. For example, Hill and Wheeler (2002) report that up to 63% of NCP is transformed to the DOC pool during the upwelling season in Oregon coastal water, owing to the decay of the phytoplankton bloom induced by the depletion of nitrate. Meador and Aluwihare (2014) also report that ~61% of NCP is partitioned into the accumulating TOC in the Amazon and Orinoco river plumes. The high DOC production from primary production is always accompanied by non-Redfield ratio uptake of carbon to nitrogen, which is demonstrated in both incubation experiments and field studies (Bury et al. 2001; Wetz and Wheeler 2003). The carbon-rich DOM accumulated in the euphotic zone may enhance carbon sequestration, once it was transported to the deep water through physical mixing and advection, or the sinking of aggregates. However, the accumulated DOM in the eutrophic layer was highly bioavailable. Compiling all the published BDOC (bioavailable DOC) data in the coastal ocean, Lønborg and Álvarez-Salgado (2012) conclude that BDOC accounts for 22% ± 12% of DOC. The export of bioavailable DOM from the coastal ocean would fuel new production and influence bacterial metabolism in the open ocean.

Partitioning of the NCP into POC is correlated with the sinking flux of POC (Eppley and Peterson 1979). Cai et al. (2015) also find a positive correlation between POC export fluxes and POC stocks on the NSCS shelf, implying that POC production in the euphotic layer could enhance the POC export. Given the estimated NCP and the production rates of TOC (DOC + POC) in the water column of the plume and upwelling zones, our mass balance showed that the removal rates of TOC were 19.9 ± 12.4 and 12.5 ± 8.1 mmol C m^{-2} d^{-1}, respectively, which accounted for 60–63% and 59% of the NCP in the plume and upwelling zones. These values were comparable or slightly higher than the previous estimates of vertical POC export flux (10.7 ± 11.6 mmol C m^{-2} d^{-1}) on the NSCS shelf during summer based on the method of 234Th: 238U disequilibria (Cai et al. 2015), indicating that sinking POC dominated the removal of TOC, and that the export flux of POC might be enhanced in the plume and upwelling zones. Our results also showed relatively high average POC production rates in the upwelling zones. However, we noted that the average removal rate of TOC in the upwelling zones was comparable to or slightly lower than that in the plume. As mentioned above, the regeneration of DIC and nutrients observed in the upwelling suggested the decomposition of POM, which may diminish the POC export flux.

Conclusions

Our observations demonstrated that DOC dynamics on the NSCS shelf, under the coinfluence of the river plume and upwelling, were jointly controlled by physical and biological forcing. Along with estimations for the net consumption of DIC and nutrients, a three end-member mixing model was used to estimate semiquantitatively the net production of DOC in this complex circulation system. DOC appeared to be autotrophic throughout the alongshore transport of the plume, while the upwelling circulation system was mixed trophic in terms of DOC net production. Nevertheless, the integrated biologically mediated DOC net production was comparable in the present river plume and upwelling system on the NSCS shelf. Both DOC and POC production in the plume and upwelling zones were significantly correlated with NCP. The partitioning of NCP into DOC was similar in the two regimes. However, the partitioning of NCP into POC was significantly higher in the upwelling zones than in the plume. Nevertheless, most portions of the NCP in the both regimes were removed from the water column through the sinking of POC. Such partitioning of the NCP in the eutrophic coastal ocean has important implications for carbon cycling in the coastal ocean.

Taken together with prior research in plume systems (Benner and Opsahl 2001; Chen and Gardner 2004; Wang et al. 2004; Meador and Aluwihare 2014), we contend that the predominant production of DOC in river-dominated shelf systems might be a ubiquitous phenomenon, likely caused by strong primary production, stimulated by abundant nutrients transported from rivers. Whether a system coinfluenced by plumes and upwelling possesses net DOC production, however, warrants a quantitative assessment, such as that presented here for the NSCS.

References

Alling, V., and others. 2010. Nonconservative behavior of dissolved organic carbon across the Laptev and East Siberian seas. Global Biogeochem. Cycles **24**: GB4033. doi:10.1029/2010GB003834

Álvarez-Salgado, X. A., M. D. Doval, and F. F. Pérez. 1999. Dissolved organic matter in shelf waters off the Ría de Vigo (NW Iberian upwelling system). J. Mar. Syst. **18**: 383–394. doi:10.1016/S0924-7963(97)00114-0

Álvarez-Salgado, X. A., J. Gago, B. M. Miguez, and F. F. Pérez. 2001. Net ecosystem production of dissolved organic carbon in a coastal upwelling system: The Ria de Vigo, Iberian margin of the North Atlantic. Limnol. Oceanogr. **46**: 135–147. doi:10.4319/lo.2001.46.1.0135

Álvarez-Salgado, X. A., J. Aristegui, E. D. Barton, and D. A. Hansell. 2007. Contribution of upwelling filaments to offshore carbon export in the subtropical Northeast Atlantic Ocean. Limnol. Oceanogr. **52**: 1287–1292. doi:10.4319/lo.2007.52.3.1287

Azam, F. 1998. Microbial control of oceanic carbon flux: The plot thickens. Science **280**: 694–696. doi:10.1126/science.280.5364.694

Bauer, J. E., and T. S. Bianchi. 2011. Dissolved organic carbon cycling and transformation, p. 7–67. *In* E. Wolanski and D. S. McLusky [eds.], Treatise on estuarine and coastal science. Academic Press.

Bauer, J. E., W. J. Cai, P. A. Raymond, T. S. Bianchi, C. S. Hopkinson, and P. A. Regnier. 2013. The changing carbon cycle of the coastal ocean. Nature **504**: 61–70. doi:10.1038/nature12857

Benner, R., and S. Opsahl. 2001. Molecular indicators of the sources and transformations of dissolved organic matter in the Mississippi river plume. Org. Geochem. **32**: 597–611. doi:10.1016/S0146-6380(00)00197-2

Bury, S. J., P. W. Boyd, T. Preston, G. Savidge, and N. J. P. Owens. 2001. Size-fractionated primary production and nitrogen uptake during a North Atlantic phytoplankton bloom: Implications for carbon export estimates. Deep-Sea Res. I **48**: 689–720. doi:10.1016/S0967-0637(00)00066-2

Cai, P. H., D. C. Zhao, L. Wang, B. Q. Huang, and M. H. Dai. 2015. Role of particle stock and phytoplankton community structure in regulating particulate organic carbon export in a large marginal sea. J. Geophys. Res. **120**: 2063–2095. doi:10.1002/2014JC010432

Cai, Y. H., L. D. Guo, X. R. Wang, A. K. Mojzis, and D. G. Redalje. 2012. The source and distribution of dissolved and particulate organic matter in the Bay of St. Louis, northern Gulf of Mexico. Estuarine Coastal Shelf Sci. **96**: 96–104. doi:10.1016/j.ecss.2011.10.017

Callahan, J., M. H. Dai, R. F. Chen, X. L. Li, Z. M. Lu, and W. Huang. 2004. Distribution of dissolved organic matter in the Pearl River Estuary, China. Mar. Chem. **89**: 211–224. doi:10.1016/j.marchem.2004.02.013

Cao, Z. M., and M. H. Dai. 2011. Shallow-depth $CaCO_3$ dissolution: Evidence from excess calcium in the South China Sea and its export to the Pacific Ocean. Global Biogeochem. Cycles **25**: GB2019. doi:10.1029/2009GB003690

Cao, Z. M., M. H. Dai, N. Zheng, D. L. Wang, Q. Li, W. D. Zhai, F. F. Meng, and J. P. Gan. 2011. Dynamics of the carbonate system in a large continental shelf system under the influence of both a river plume and coastal upwelling. J. Geophys. Res. **116**: G02010. doi:10.1029/2010JG001596

Carlson, C. A., H. W. Ducklow, and A. F. Michaels. 1994. Annual flux of dissolved organic carbon from the euphotic zone in the northwestern Sargasso Sea. Nature **371**: 405–408. doi:10.1038/371405a0

Carlson, C. A., H. W. Ducklow, D. A. Hansell, and W. O. Smith, Jr. 1998. Organic carbon partitioning during spring phytoplankton blooms in the Ross Sea polynya and the Sargasso Sea. Limnol. Oceanogr. **43**: 375–386. doi:10.4319/lo.1998.43.3.0375

Carlson, C. A., D. A. Hansell, E. T. Peltzer, and W. O. Smith, Jr. 2000. Stocks and dynamics of dissolved and particulate organic matter in the southern Ross Sea, Antarctica. Deep-Sea Res. II **47**: 3201–3225. doi:10.1016/S0967-0645(00)00065-5

Carlson, C. A., and D. A. Hansell. 2015. DOM sources, sinks, reactivity, and budgets, p. 65–90. *In* D. A. Hansell and C. A. Carlson [eds.], Biogeochemistry of marine dissolved organic carbon. Academic Press.

Casareto, B. E., M. P. Niraula, and Y. Suzuki. 2012. Dynamics of organic carbon under different inorganic nitrogen levels and phytoplankton composition. Estuarine Coastal Shelf Sci. **102-103**: 84–94. doi:10.1016/j.ecss.2012.03.019

Chen, C. T. A. 2003. New vs. export production on the continental shelf. Deep-Sea Res. II **50**: 1327–1333. doi:10.1016/S0967-0645(03)00026-2

Chen, R. F., and G. B. Gardner. 2004. High-resolution measurements of chromophoric dissolved organic matter in the Mississippi and Atchafalaya River plume regions. Mar. Chem. **89**: 103–125. doi:10.1016/j.marchem.2004.02.026

Chen, W. F. 2008. On the export fluxes, seasonality and controls of particulate organic carbon in the Northern South China Sea. Ph.D. thesis, Xiamen Univ.

Cifuentes, L. A., J. H. Sharp, and M. L. Fogel. 1988. Stable carbon and nitrogen isotope biogeochemistry in the Delaware Estuary. Limnol. Oceanogr. **33**: 1102–1115. doi:10.4319/lo.1988.33.5.1102

Dai, M. H., and others. 2008*a*. Effects of an estuary plume-associated bloom on the carbonate system in the lower reaches of the Pearl River estuary and the coastal zone of the northern South China Sea. Cont. Shelf Res. **28**: 1416–1423. doi:10.1016/j.csr.2007.04.018

Dai, M. H., L. F. Wang, X. H. Guo, W. D. Zhai, Q. Li, B. Y. He, and S. J. Kao. 2008*b*. Nitrification and inorganic nitrogen distribution in a large perturbed river/estuarine system: The Pearl River Estuary, China. Biogeosciences **5**: 1227–1244. doi:10.5194/bg-5-1227-2008

Dai, M. H., and others. 2009. Excess total organic carbon in the intermediate water of the South China Sea and its export to the North Pacific. Geochem. Geophys. Geosyst. **10**: 1029–1020, Q12002. doi:10.1029/2009GC002752

Dai, M. H., Z. Q. Yin, F. F. Meng, Q. Liu, and W. J. Cai. 2012. Spatial distribution of riverine DOC inputs to the ocean: An updated global synthesis. Curr. Opin. Environ. Sustain. **4**: 170–178. doi:10.1016/j.cosust.2012.03.003

Dai, M. H., J. P. Gan, A. Q. Han, H. S. Kung, and Z. Yin. 2014. Physical dynamics and biogeochemistry of the Pearl River plume, p. 325–335. *In* T. Bianchi, M. Allison, and W. J. Cai. [eds.], Biogeochemical dynamics at major river-coastal interfaces. Cambridge Univ. Press.

Doval, M. D., X. A. Álvarez-Salgado, and F. F. Pérez. 1997. Dissolved organic matter in a temperate embayment affected by coastal upwelling. Mar. Ecol. Prog. Ser. **157**: 21–37. doi:10.3354/meps157021

Engel, A., S. Goldthwait, U. Passow, and A. Alldredge. 2002. Temporal decoupling of carbon and nitrogen dynamics in

a mesocosm diatom bloom. Limnol. Oceanogr. **47**: 753–761. doi:10.4319/lo.2002.47.3.0753

Eppley, R. W., and B. J. Peterson. 1979. Particulate organic matter flux and planktonic new production in the deep ocean. Nature **282**: 677–680. doi:10.1038/282677a0

Gan, J. P., L. Li, D. X. Wang, and X. G. Guo. 2009*a*. Interaction of a river plume with coastal upwelling in the northeastern South China Sea. Cont. Shelf Res. **29**: 728–740. doi:10.1016/j.csr.2008.12.002

Gan, J. P., A. Cheung, X. G. Guo, and L. Li. 2009*b*. Intensified upwelling over a widened shelf in the north eastern South China Sea. J. Geophys. Res. **114**: C09019. doi:10.1029/2007JC004660

Gan, J. P., Z. M. Lu, M. H. Dai, A. Y. Y. Cheung, H. B. Liu, and P. Harrison. 2010. Biological response to intensified upwelling and to a river plume in the northeastern South China Sea: A modeling study. J. Geophys. Res. **115**: C09001. doi:10.1029/2009JC005569

Gattuso, J. P., M. Frankignoulle, and R. Wollast. 1998. Carbon and carbonate metabolism in coastal aquatic ecosystems. Annu. Rev. Ecol. Syst. **29**: 405–434. doi:10.1146/annurev.ecolsys.29.1.405

Guo, X. H., M. H. Dai, W. D. Zhai, W. J. Cai, and B. S. Chen. 2009. CO_2 flux and seasonal variability in a large subtropical estuarine system, the Pearl River Estuary, China. J. Geophys. Res. **114**: G03013. doi:10.1029/2008JG000905

Guo, X. H., W. D. Zhai, M. H. Dai, C. Zhang, Y. Bai, Y. Xu, Q. Li, and G. Z. Wang. 2015. Air-sea CO2 fluxes in the East China Sea based on multiple-year underway observations. Biogeosciences **12**: 5495–5514. doi:10.5194/bg-12-5495-2015

Halewood, E. R., C. A. Carlson, M. A. Brzezinski, D. C. Reed, and J. Goodman. 2012. Annual cycle of organic matter partitioning and its availability to bacteria across the Santa Barbara Channel continental shelf. Aquat. Microb. Ecol. **67**: 189–209. doi:10.3354/ame01586

Han, A. Q., M. H. Dai, S. J. Kao, J. P. Gan, Q. Li, L. F. Wang, W. D. Zhai, and L. Wang. 2012. Nutrient dynamics and biological consumption in a large continental shelf system under the influence of both a river plume and coastal upwelling. Limnol. Oceanogr. **57**: 486–502. doi:10.4319/lo.2012.57.2.0486

Hansell, D. A. 2013. Recalcitrant dissolved organic carbon fractions. Annu. Rev. Mar. Sci. **5**: 421–445. doi:10.1146/annurev-marine-120710-100757

Hansell, D. A., and C. A. Carlson. 1998. Net community production of dissolved organic carbon. Global Biogeochem. Cycles **12**: 443–453. doi:10.1029/98GB01928

Hansell, D. A., and E. T. Peltzer. 1998. Spatial and temporal variations of total organic carbon in the Arabian Sea. Deep-Sea Res. II **45**: 2171–2193. doi:10.1016/S0967-0645(98)00067-8

Hansell, D. A., and C. A. Carlson. 2001. Maine dissolved organic matter and carbon cycle. Oceanography **14**: 41–49. doi:10.5670/oceanog.2001.05

He, B. Y., and others. 2010. Distribution, degradation and dynamics of dissolved organic carbon and its major compound classes in the Pearl River estuary, China. Mar. Chem. **119**: 52–64. doi:10.1016/j.marchem.2009.12.006

Hill, J. K., and P. A. Wheeler. 2002. Organic carbon and nitrogen in the northern California Current system: Comparison of offshore, river plume and coastally upwelled waters. Prog. Oceanogr. **53**: 369–387. doi:10.1016/S0079-6611(02)00037-X

Jurado, E., J. Dachs, C. M. Duarte, and R. Simo. 2008. Atmospheric deposition of organic and black carbon to the global oceans. Atmos. Environ. **42**: 7931–7939. doi:10.1016/j.atmosenv.2008.07.029

Li, J. N., C. F. Yang, F. Z. Li., Q. He, and W. Li. 2013. A comparison of summer precipitation structures over the South China Sea and the East China Sea based on tropical rainfall measurement mission. Acta Oceanol. Sin. **32**: 41–49. doi:10.1007/s13131-013-0376-3

Li, W. B., C. Luo, D. X. Wang, and T. Lei. 2010. Diurnal variations of precipitation over the South China Sea. Meteorol. Atmos. Phys. **109**: 33–46. doi:10.1007/s00703-010-0094-8

Liu, K. K., S. J. Kao, L. S. Wen, and K. L. Chen. 2007. Carbon and nitrogen isotopic compositions of particulate organic matter and biogeochemical processes in the eutrophic Danshuei Estuary in northern Taiwan. Sci. Total Environ. **382**: 103–120. doi:10.1016/j.scitotenv.2007.04.019

Liu, Q., M. H. Dai, W. F. Chen, C. A. Huh, G. Wang, and M. A. Charette. 2012. How significant is submarine groundwater discharge and its associated dissolved inorganic carbon in a river-dominated shelf system? Biogeosciences **9**: 1777–1795. doi:10.5194/bg-9-1777-2012

Lomas, M. W., and N. R. Bates. 2004. Potential controls on interannual partitioning of organic carbon during the winter/spring phytoplankton bloom at the Bermuda Atlantic time-series study (BATS) site. Deep-Sea Res. Part I **51**: 1619–1636. doi:10.1016/j.dsr.2004.06.007

Lønborg, C., X. A. Álvarez-Salgado, S. Martínez-García, A. E. J. Miller, and E. Teira. 2010. Stoichiometry of dissolved organic matter and the kinetics of its microbial degradation in a coastal upwelling system. Aquat. Microb. Ecol. **58**: 117–126. doi:10.3354/ame01364

Lønborg, C., and X. A. Álvarez-Salgado. 2012. Recycling versus export of bioavailable dissolved organic matter in the coastal ocean and efficiency of the continental shelf pump. Global Biogeochem. Cycles **26**: GB3018. doi:10.1029/2012GB004353

Meador, T. B., and L. I. Aluwihare. 2014. Production of dissolved organic carbon enriched in deoxy sugars representing an additional sink for biological C drawdown in the Amazon River plume. Global Biogeochem. Cycles **28**: 1149–1161. doi:10.100 2/2013GB004778

Shen, Y., C. G. Fichot, and R. Benner. 2012. Dissolved organic matter composition and bioavailability reflect

ecosystem productivity in the Western Arctic Ocean. Biogeosciences **9**: 4993–5005. doi:10.5194/bg-9-4993-2012

Shu, Y. Q., J. Zhu, D. X. Wang, and X. J. Xiao. 2011. Assimilating remote sensing and in situ observations into a coastal model of northern South China Sea using ensemble Kalman filter. Cont. Shelf Res. **31**: S24–S26. doi:10.1016/j.csr.2011.01.017

Smith, D. C., M. Simon, A. L. Alldredge, and F. Azam. 1992. Intense hydrolytic enzyme activity on marine aggregates and implications for rapid particle dissolution. Nature **359**: 139–142. doi:10.1038/359139a0

Wang, X. C., R. F. Chen, and B. Gardner. 2004. Sources and transport of dissolved and particulate organic carbon in the Mississippi River estuary and adjacent coastal waters of the northern Gulf of Mexico. Mar. Chem. **89**: 241–256. doi:10.1016/j.marchem.2004.02.014

Wear, E. K., C. A. Carlson, A. K. James, M. A. Brzezinski., L. A. Windecker, and C. E. Nelson. 2015. Synchronous shifts in dissolved organic carbon bioavailability and bacterial community responses over the course of an upwelling-driven phytoplankton bloom. Limnol. Oceanogr. **60**: 657–677. doi:10.1002/lno.10042

Wetz, M. S., and P. A. Wheeler. 2003. Production and partitioning of organic matter during simulated phytoplankton blooms. Limnol. Oceanogr. **48**: 1808–1817. doi:10.4319/lo.2003.48.5.1808

Williams, P. J. L. B. 1995. Evidence for the seasonal accumulation of carbon-rich dissolved organic matter, its scale in comparison with changes in particulate material and the consequential effects on net C/N assimilation ratios. Mar. Chem. **51**: 17–29. doi:10.1016/0304-4203(95)00046-T

Wollast, R. 1998. Evaluation and comparison of the global carbon cycle in the coastal zone and in the open ocean, p. 213–252. *In* K. H. Brink and A. R. Robinson [eds.], The global coastal ocean. John Wiley & Sons.

Wu, K., M. H. Dai, J. H. Chen, F. F. Meng, X. L. Li, Z. Y. Liu, C. J. Du, and J. P. Gan. 2015. Dissolved organic carbon in the South China Sea and its exchange with the Western Pacific Ocean. Deep-Sea Res. II **122**: 41–51. doi:10.1016/j.dsr2.2015.06.013

Zhou, K. B., M. H. Dai, S. J. Kao, L. Wang, P. Xiu, F. Cai, J. W. Tian, and Y. Liu. 2013. Apparent enhancement of 234Th-based particle export associated with anticyclonic eddies. Earth Planet. Sci. Lett. **381**: 198–209. doi:10.1016/j.epsl.2013.07.039

Acknowledgments

We thank the captain and the crew of *R/V Shiyan III* for their cooperation during the cruise; Dongxiao Wang and Jianyu Hu for providing the CTD data; Nana Wu is acknowledged for help with POC sampling during the cruise; and Jingyu Yang and Shu-Ji Kao for their help with POC sample measurements. Professor John Hodgkiss is thanked for his help with English. This research was funded by the National Basic Research Program of China (973 Program) through grants 2015CB954000 and the National Natural Science Foundation of China through grants 41361164001, 91328202, 41130857, and 91428308.

Conflict of Interest

None declared.

Submitted 23 June 2016
Revised 11 October 2016
Accepted 17 October 2016

Associate editor: Ronnie Glud